# DESIGN OF A DISTRIBUTED TERAHERTZ PHOTOMIXER

E. K. Duerr[1], K. A. McIntosh, and S. Verghese
Lincoln Laboratory, Massachusetts Institute of Technology
Lexington, MA 02420

**Abstract**

Photomixers generate coherent radiation at the difference frequency of two lasers by performing optical heterodyne conversion in low-temperature-grown (LTG) GaAs. Antenna coupled photomixers have been demonstrated as local oscillators (LO) up to 630 GHz [1] and have produced power up to 5 THz [2]. Using a distributed photomixer structure may increase output power at high frequencies. The distributed photomixer consists of coplanar strips (CPS) fabricated on top of a dielectric ridge waveguide that guides the combined output of two diode lasers. The conductance of a thin layer of LTG-GaAs between the CPS and optical guide is modulated by the evanescently coupled optical beat signal. To collect the photocurrent and to velocity match the THz and optical waves, the CPS are periodically loaded with thin electrodes. The CPS are terminated in a planar antenna that efficiently radiates the THz wave guided by the CPS.

## 1 Introduction

Photomixers generate coherent radiation at the difference frequency of two lasers by performing optical heterodyne conversion in low-temperature-grown (LTG) GaAs. LTG-GaAs is an ultrafast photoconductor with carrier lifetime measured to be less than 200 fs [3], which gives the photomixer an extremely high intrinsic bandwidth. In previously demonstrated photomixers, a dc-biased LTG-GaAs switch is modulated by the optical beat signal of the beam-combined output of two lasers operating at slightly different frequencies [4, 5]. The metal lines which provide the dc-bias also act as the RF structure which couples the THz radiation out of the LTG-GaAs switch [6]. In addition to being demonstrated as an LO, photomixers have been used for time-domain [7] and frequency-domain [8, 9, 10] THz spectroscopy.

Using a distributed photomixer structure may increase the output power at high frequencies and provide a broader bandwidth than current "lumped-element" designs. Current designs exhibit a frequency roll-off component from the antenna resistance and capacitance of the LTG-GaAs switch. A distributed photomixer based on an active transmission line can

[1]electronic mail: duerr@alum.mit.edu

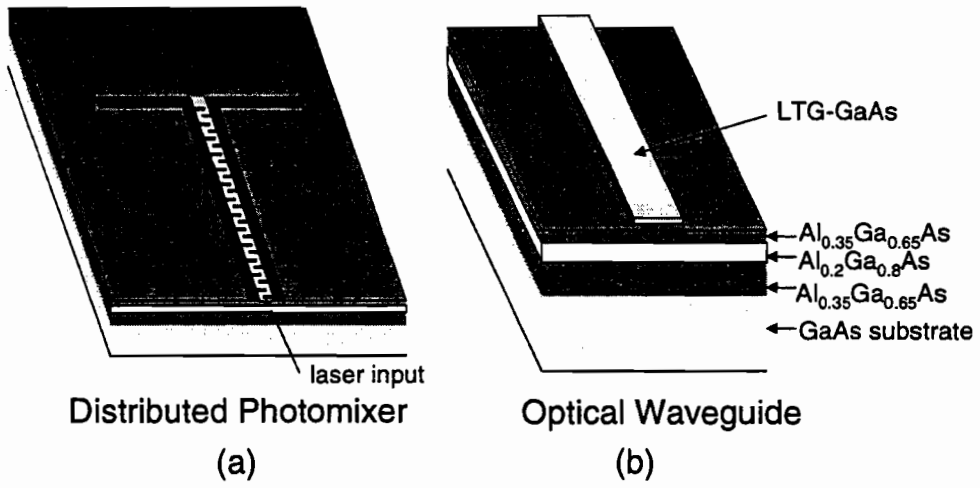


Figure 1: (a) Schematic of the distributed photomixer showing the periodically loaded cps waveguide, dipole antenna and optical waveguide. (b) Detail of optical waveguide showing LTG-GaAs absorber layer.

eliminate this roll-off. A second frequency-roll-off component is due to the finite photocarrier lifetime and is intrinsic to the material. Additionally, because the primary failure mode of photomixers is through excess thermal heating of the photomixer by the pump lasers [11], a distributed structure would mitigate this problem by causing the laser power to be absorbed in a much larger area.

## 2 Distributed Photomixer Design

The distributed photomixer shown in Figure 1 (a) consists of coplanar strips (CPS) fabricated on top of a dielectric ridge waveguide that guides the combined output of two diode lasers. The conductance of a thin layer of LTG-GaAs between the CPS and optical guide is modulated by the evanescently coupled optical beat signal. The THz conductance wave between the dc-biased CPS creates a THz electromagnetic wave which propagates along the CPS. To velocity match the THz and optical waves, the coplanar strips are periodically loaded with thin electrodes that add a small shunt capacitance to the line. The CPS are terminated in a planar antenna that efficiently radiates the THz wave.

## 2.1 Dielectric Waveguide Design

The dielectric waveguide must be designed so that the optical signal is weakly coupled to the absorbing LTG-GaAs layer. Weak coupling ensures that optical power is absorbed over a long distance ($\sim 150\,\mu$m) and that the thermal load is distributed. Weak coupling also allows the optical guide and THz guide to be analyzed separately. Confinement of the optical mode in the plane of the wafer is provided by layers of $Al_xGa_{1-x}As$ with different Al and Ga fractions. Lateral confinement is provided by a strip etched from the upper cladding layer of the waveguide as shown in Figure 1 (b). The strip-loaded waveguide provides the weak lateral confinement necessary to guide a single optical mode.

The dielectric ridge waveguide was analyzed with the effective index method to yield mode propagation constants. With these values, the mode profile was calculated and the fraction of power in each part of the waveguide was calculated. This information leads to an estimate of the absorption coefficient and, therefore, the extinction length of the optical mode—the length at which the remaining optical power is 37% ($e^{-1}$) of the incident power.

For the first generation of devices, the dielectric stack consists of a 5000-Å-thick $Al_{0.2}Ga_{0.8}As$ core ($n = 3.38$) grown on top of 3.5 $\mu$m of $Al_{0.35}Ga_{0.65}As$ ($n = 3.33$). The upper cladding is formed by 2500Å of $Al_{0.35}Ga_{0.65}As$ followed by 1000Å of LTG-GaAs of absorber. A ridge height of 2500Å produces a mode which is approximately 1$\mu$m by 3$\mu$m and has 0.15% of the mode in the LTG-GaAs absorbing layer. The predicted extinction length for this geometry is 90$\mu$m. The effective index seen by the optical mode is $n_{eff} = 3.35$.

## 2.2 THz Waveguide Design

Coplanar strips (CPS) fabricated on top of the ridge waveguide perform the dual function of providing the dc-bias for the LTG-GaAs photoconductor and guiding the THz signal. Because the velocity of the THz signal (0.38c) is higher than the group velocity of the optical signal (0.3c), the CPS must be periodically loaded with thin electrodes to slow the THz signal and velocity match it to the optical signal for optimum power transfer [12].

Quasi-static electromagnetic models provided an initial estimate for the CPS dimensions required for a particular impedance [13]. Because the LTG-GaAs is very high impedance under constant wave (cw) illumination, the photoconductor can be considered a current source. Therefore, assuming a matched antenna impedance, the output power is linearly related to the CPS impedance. However, for high values of CPS impedance the lines become very narrow and thus excessively lossy. For our first generation of devices, the CPS consist of 3.2-$\mu$m-wide strips separated by a 3 $\mu$m gap. The calculated impedance of the line was 90 $\Omega$ before being

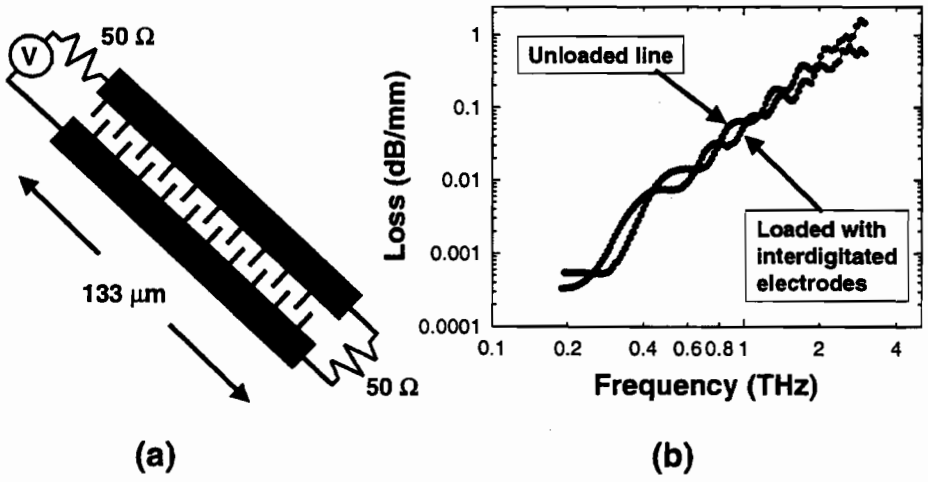


Figure 2: (a) The circuit used to determine radiation loss from a method-of-moments calculation. (b) Calculated radiation loss for CPS with and without interdigitated electrodes.

loaded with interdigitated electrodes.

The spacing and dimensions of the thin electrodes periodically loading the CPS are critical for determining the velocity of the THz wave. Quasi-static models [14] are useful for initial estimates for electrode dimensions, but a more accurate model is desirable. More precise dimensions were calculated using Hewlett Packard's electromagnetic field solver for planar circuits, Momentum [15]. Perfect metal conductors were assumed in all the calculations. Quasi-static calculations predicted that 2.1-$\mu$m-long electrodes spaced by 0.6 $\mu$m provide optimal velocity matching. Momentum calculations revised those dimensions to 2.0-$\mu$m-long electrodes spaced by 0.8 $\mu$m. The impedance of the line at 1.5 THz as modified by the presence of the electrodes is 76 $\Omega$ according to Momentum and 72 $\Omega$ according to quasi-static calculations. The loaded CPS impedance varies from 78 $\Omega$ at 170 GHz to 72 $\Omega$ at 2.4 THz.

The variation in impedance with frequency can be attributed to radiation loss, which describes attenuation of the THz wave through unwanted radiation into the substrate. To calculate the radiation loss, the $S$-parameters of the two-port network shown in Figure 2(a) were calculated using the method-of-moments code, Momentum. By comparing the power transmitted from the source to the power absorbed in the load, the power loss due to radiation was calculated. The results for an unloaded CPS line and for a CPS line loaded with electrodes for optimal velocity matching are shown in Figure 2(b). The radiation loss remains less than

Table 1: *Planar Antenna Designs*

| Frequency [THz] | Length prediction from [17] [$\lambda_o$] | Momentum length prediction [$\lambda_o$] | Width [$\mu$m] | $Z_{ant}$ [$\Omega$] |
|---|---|---|---|---|
| 0.85 | 0.18 | 0.20 | 2 | 37 |
| 1.6 | 0.18 | 0.22 | 1.5 | 41 |
| 2.5 | 0.17 | 0.24 | 1.5 | 44 |

2 dB/mm up to 3 THz and is cubic with frequency as expected from closed-form approximations [16]. The interdigitated electrodes do not introduce significant loss below 3 THz. Oscillations in the data can be attributed to standing wave effects that are significant in the short length of line used in the calculations.

In order to test the CPS modeling, three different electrode geometries were designed: 1) no electrodes, 2) theoretically optimal electrode dimensions which add the correct capacitance $\left(0.06\frac{\text{fF}}{\mu\text{m}}\right)$, and 3) electrodes with a 0.4$\mu$m gap and 2.3$\mu$m length which add $0.1\frac{\text{fF}}{\mu\text{m}}$. The first fabrication run of distributed photomixers included these three designs for CPS.

## 2.3 Antenna Design

A planar antenna at the end of the active area of the CPS radiates the THz wave. Two types of antennas were designed and fabricated, bowtie antennas and resonant half-wave dipoles. The bandwidth of the transmission line structure will be measured by terminating the CPS in a broadband bowtie antenna structure. Resonant half-wave dipoles have superior radiation patterns and better polarization performance than bowtie antennas. Therefore, dipoles were designed for 850 GHz, 1.6 THz, and 2.5 THz. Initial estimates for dipole dimensions were obtained from [17] and were revised using Momentum. Table 1 lists dimensions for the dipole antennas. Lengths deviate more from the calculations in [17] as frequency increases, because the 3$\mu$m gap between the CPS feeding the dipole becomes a larger fraction of the free-space wavelength $\lambda_0$.

## 2.4 Performance Estimates

By combining the data from these analyses with experimentally obtained data for photoconductance and carrier lifetime in a SPICE circuit model, photomixer performance is quantitatively predicted. An approximate model of the distributed photomixer is formed by cascading one hundred segments of the discrete circuit shown in Figure 3, where each segment represents an incremental length of the optical or THz guides. Each segment of the THz CPS model

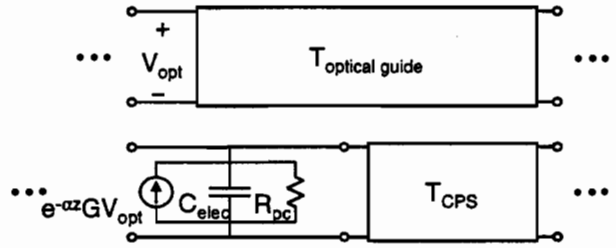


Figure 3: One segment of a SPICE circuit model for the distributed photomixer. The upper section is the optical guide model. The lower section is the THz CPS model.

Table 2: *Distributed Photomixer Performance. Values indicate fraction of power available compared to optimal velocity match* ($C_{added} = 0.06\frac{fF}{\mu m}$).

| $C_{added}$ [fF/$\mu$m] | Frac. $P_{opt}$ at 1 THz | Frac. $P_{opt}$ at 1.5 THz | Frac. $P_{opt}$ at 2 THz | Frac. $P_{opt}$ at 2.5 THz |
|---|---|---|---|---|
| 0 | 1.0 | 0.67 | 0.33 | 0.17 |
| 0.048 | 1.0 | 1.0 | 0.95 | 0.90 |
| 0.072 | 0.90 | 0.87 | 0.87 | 0.83 |
| 0.10 | 0.70 | 0.57 | 0.50 | 0.33 |

consists of a transmission line segment to model the CPS, a lumped capacitor to model the thin electrodes, a resistor to model losses in the photoconductor, and a voltage-dependent current source to model the current generated by the biased photoconductor. The voltage upon which the current source depends is the voltage at the corresponding segment along the optical guide circuit model. This voltage represents the optical intensity at the corresponding point along the real optical guide. The scaling factors are the experimentally determined photoconductance and an attenuation factor to model diminishing optical power in the optical guide. The simulations predict output power of 8$\mu$W at 1.7 THz and 4$\mu$W at 2.4 THz.

To demonstrate the dependence of power on velocity matching, the distributed photomixer was simulated with different values of distributed capacitance added by the periodic thin electrodes. Table 2 shows the fraction of power available for 4 cases: 1) no electrodes, 2) $0.8C_{optimal}$, 3) $1.2C_{optimal}$, and 4) added capacitance corresponding to a gap of 0.4$\mu$m and length of 2.3$\mu$m. A power bandwidth plot for cases 1 and 4 as well as the optimal velocity matched design are shown in Figure 4. These three designs were normalized to have the same overall dc photoconductance.

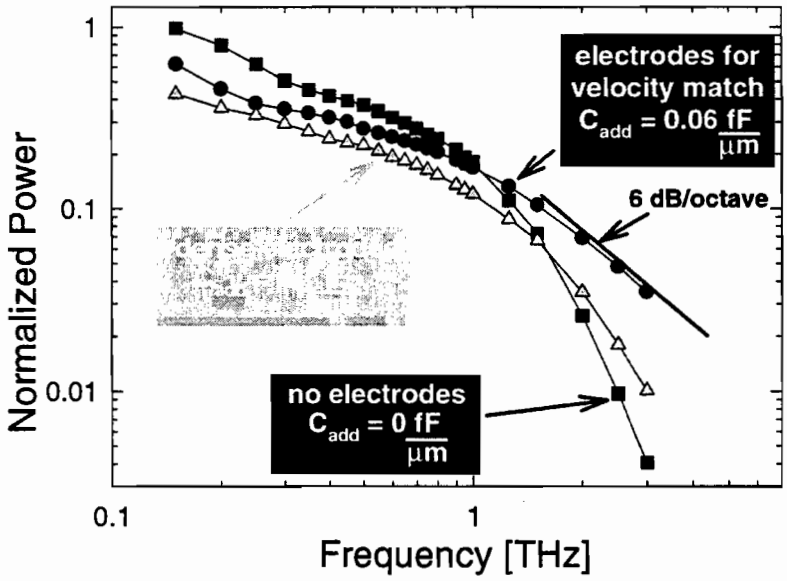


Figure 4: Power bandwidth plot for the distributed photomixer structure comparing the performance the an optimal velocity-matched structure to a structure with no electrodes and a structure with dense electrodes (case 4 in Table 2).

# 3 Conclusions

Distributed photomixers have been designed to overcome the limitations of current photomixer designs and provide higher power over a larger bandwidth. Through a combination of analytical and numerical techniques, the performance of distributed structures has been modeled as a function of several design parameters.

# References

[1] E. K. Duerr, K. A. McIntosh, S. M. Duffy, S. D. Calawa, S. Verghese, C.-Y. E. Tong, R. Kimberk, R. Blundell, *to appear in Proc. 1999 IEEE MTT Intl. Micro. Symp.* (1999).

[2] K. A. McIntosh, E. R. Brown, K. B. Nichols, O. B. McMahon, W. F. DiNatale, and T. M. Lyszczarz, *Appl. Phys. Lett.* **67**, 3844 (1995).

[3] K. A. McIntosh, K. B. Nichols, S. Verghese, E. R. Brown, *Appl. Phys. Lett.* **70**, 354 (1997).

[4] S. Matsuura, G. Blake, P. Chen, J. C. Pearson, H. M. Pickett, *Proc. 9th Intl. Symp. on Space THz Tech.* 445 (1998).

[5] S. Verghese, K. A. McIntosh, and E. R. Brown, *IEEE Trans. Micro. Theory Tech.* **45**, 1301 (1997).

[6] K. A. McIntosh, E. R. Brown, K. B. Nichols, O. B. McMahon, W. F. Dinatale, and T. M. Lyszczarz, *Appl. Phys. Lett.* **69**, 3632 (1996).

[7] M. Tani, S. Matsuura, K. Sakai, *J. Comm. Res. Lab.* **43** 151 (1996).

[8] S. Verghese, K. A. McIntosh, S. Calawa, W. F. Dinatale, E. K. Duerr, K. A. Molvar, *Appl. Phys. Lett.* **73**, 3824 (1998).

[9] P. Chen, G. A. Blake, M. C. Gaidis, E. R. Brown, K. A. McIntosh, S. Y. Chou, M. I. Nahan, and F. Williamson, *Appl. Phys. Lett.* **71**, 1601 (1997).

[10] A. S. Pine, R. D. Suenram, E. R. Brown, K. A. McIntosh, *J. of Molec. Spect.* **175**, 37 (1996).

[11] S. Verghese, K. A. McIntosh, and E. R. Brown, *Appl. Phys. Lett.* **71**, 2743 (1997).

[12] L. Y. Lin, M. C. Wu, T. Itoh, T. A. Vang, R. E. Muller, D. L. Sivco, and A. Y. Cho, *IEEE Trans. Micro. Theory Tech.* **45**, 1320 (1997).

[13] K. C. Gupta, R. Garg, I. Bahl, P. Bhartia, *Microstrip Lines and Slotlines*, Boston: Artech House, Ch. 7, 1996.

[14] Y. C. Lim and R. A. Moore, *IEEE Trans. Elec. Dev.* **ED-15**, 173 (1968).

[15] MOMENTUM, method-of-moments solver for planar conductors. Hewlett-Packard EEsof division, 5301 Stevens Creek Blvd., Santa Clara, CA 95052-8059.

[16] M. Y. Frankel, S. Gupta, J. A. Valdmanis, G. A. Mourou. *IEEE Trans. Micro. Theory Tech.* **39**, 910 (1991).

[17] M. Kominami, D. M. Pozar, and D. H. Schaubert, *IEEE Trans. Ant. and Prop.* **33**, 600 (1985).